Journal of Archaeological Science: Reports 67 (2025) 105370

Contents lists available at ScienceDirect

Journal of Archaeological Science: Reports

journal homepage: www.elsevier.com/locate/jasrep

Provenance and selective quarrying of New Kingdom Nubian sandstones on Sai Island, Sudan: Insights from ilmenite alterations and matrix compositions

Fabian Dellefant [a,*], Rosemarie Klemm [a], Julia Budka [a], Melanie Kaliwoda [b,c]

[a] Department of Cultural and Ancient Studies, Ludwig-Maximilians-Universität München, Katharina-von-Bora-Str. 10, 80333 Munich, Germany
[b] Department of Earth and Environmental Sciences, Ludwig-Maximilians-Universität München, Theresienstr. 41, 80333 Munich, Germany
[c] Mineralogical State Collection Munich (MSM), Bavarian Natural History Collections (SNSB), Theresienstr. 41, 80333 Munich, Germany

ARTICLE INFO

Keywords:
Nubian sandstone
Sudan
Sai Island
Provenance analysis
Ilmenite alteration series
Raman spectroscopy

ABSTRACT

This study examines the mineralogical composition and alteration products of ilmenite and the matrix in Nubian sandstones from Temple A and ancient quarries on Sai Island (northern Sudan) for insights into their provenance. We characterized the grains and their diagenetic alteration products via polarized light microscopy, scanning electron microscopy (SEM), and Raman spectroscopy. All samples, deriving from Late Bronze Age contexts (c. 15th–14th cent. BCE), are dominated by quartz (>90 %), minor feldspar (<10 %), and rare lithoclasts (<5%). Depending on the amount of matrix (5–50 %), the sandstones are classified as quartz arenites or quartz wackes. Generally, temple sandstones are moderately sorted, smaller-grained (250 μm to 310 μm), and lighter colored, compared to quarry samples, which are (very) poorly sorted, larger-grained (190 μm to 750 μm), and darker. All sandstone samples bear ilmenite alteration products (pseudorutile, rutile, anatase, hematite, Fe-hydroxides) and have matrices composed of kaolinite and illite, indicating similar weathering, diagenetic, and burial histories. The grains derive from a pluton and the Fe-Ti-oxide assemblage before alteration was consistently ilmenite with minor rutile and hematite, which suggests a late-stage magmatic source with comparable temperature and oxygen fugacity conditions for all samples. The results indicate that all investigated samples likely originate from the same or closely related stratigraphic units. The mineralogical homogeneity precludes precise attribution of temple blocks to specific quarries, however, the difference between moderately sorted temple and (very) poorly sorted quarry sandstones could be explained by selective quarrying by ancient builders to ensure aesthetic and material consistency in construction.

1. Introduction

Sai Island is located in northern Sudan covering an area of about 32 km^2, between the 2nd and 3rd Nile cataracts (Fig. 1a). The considerable time-depth of evidence for human activity on Sai Island, starting with the late Early Paleolithic (Van Peer et al., 2003), showcases the prominence of the area. The geology of Sai Island comprises several types of metamorphic Precambrian rocks and Nubian sandstone, most of which are covered by thin layers of comparatively much younger Nile sediments (Budka, 2024, p.27, 2020, p.29; Van Peer et al., 2003). Quartz sandstone was generally the preferred Pharaonic building material along the Nile Valley, from Esna in Upper Egypt to Jebel Barkal close to the 4th cataract (Budka, 2020, p.42; Klemm and Klemm, 2008, 2001). During the 18th Egyptian Dynasty (c. 1550–1292 BCE), a fortified Pharaonic town was founded on the northeastern bank of Sai Island, and this is invaluable to our understanding of the relationships between Egyptians and Nubians during the Egyptian colonial era in Nubia (Budka, 2020, 2017 and references therein).

Several variants of Nubian sandstone — the most common rock identified on Sai Island — were documented by the European Research Council (ERC)-funded AcrossBorders Project (Budka, 2020, pp. 42-52; Draganits, 2014). One of the most important results of the project was locating potential sources for the stones used in New Kingdom buildings on Sai Island, especially for the 18th Dynasty sanctuary of Temple A. The general location of sandstone quarries on Sai Island had previously been suggested as being to the north and south of the Ottoman fortress which

* Corresponding author.
E-mail address: fabian.dellefant@lmu.de (F. Dellefant).

https://doi.org/10.1016/j.jasrep.2025.105370
Received 13 May 2025; Received in revised form 18 August 2025; Accepted 21 August 2025
Available online 13 October 2025

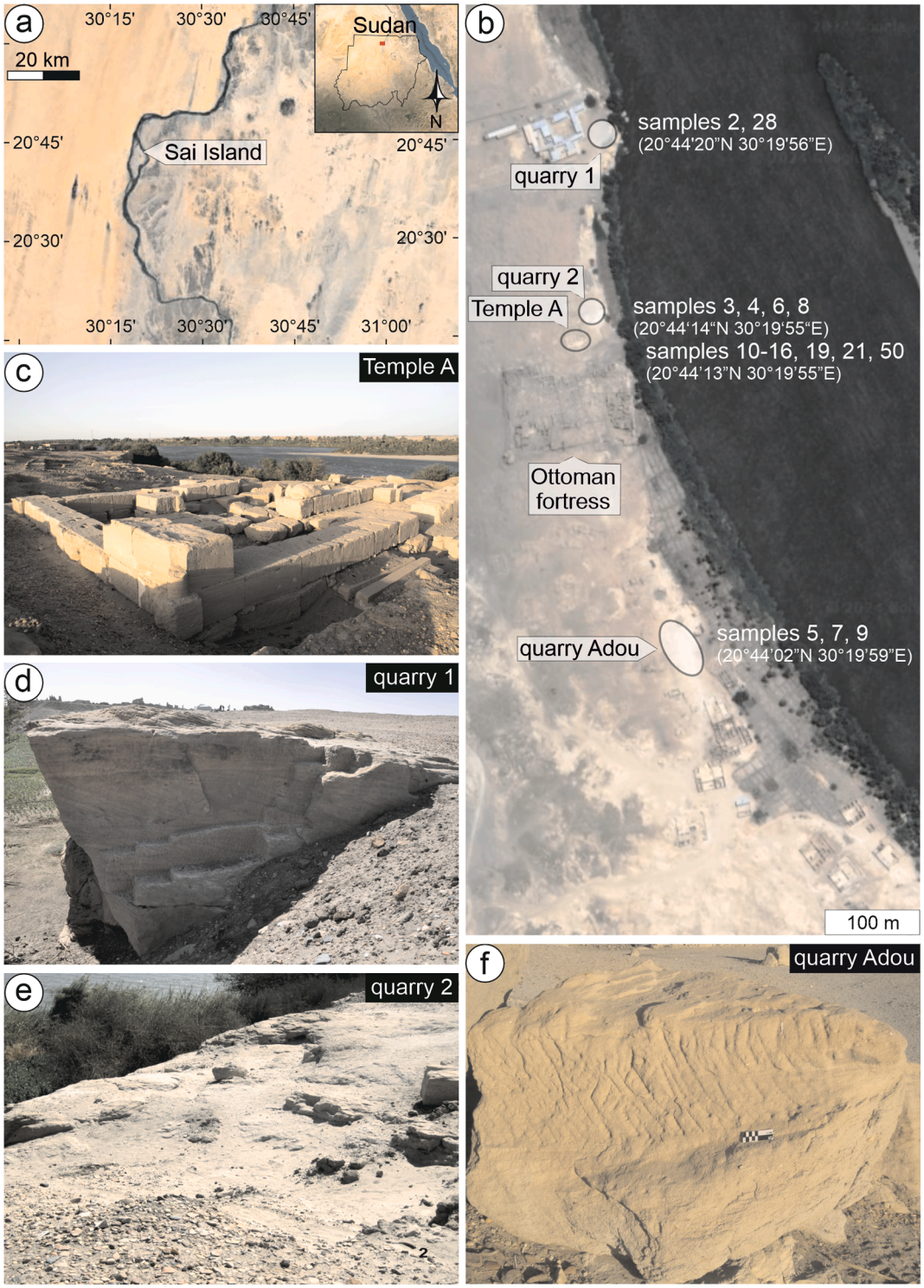

Fig. 1. a) Map of the Nile River in northern Sudan (Northeast Africa) showing the location of Sai Island (Inset: Panos Kratimenos, DiverseNile project). **b)** Sampling areas of Temple A and the ancient quarries with respective sample names and coordinates adjacent to the Ottoman fortress. (a,b) modified from Google Earth. Field photos of **c)** Temple A debris, ancient **d)** quarry 1, **e)** quarry 2, and **f)** quarry Adou, where ancient tool marks are still preserved. Photo (c) modified from Ingrid Adenstedt (copyright AcrossBorders).

overlies the southern area of the New Kingdom town (Vercoutter, 1986, pp. 8-10, 1958, p. 147). Thanks to preparatory research (especially with lithologically processed Landsat TM images) and on-site research by Dietrich and Rosemarie Klemm, seven sandstone quarries near the New Kingdom town were identified in 2016 (Budka, 2024, pp. 27-28 and references therein). Two of these sandstone quarries (quarry sites 1 & 2; Fig. 1b, d, e) are located just east of the town wall and, as such, would have been the most conveniently placed for building materials used in the town. Preliminary petrographic analysis by the AcrossBorders Project (Budka, 2020, pp. 42-52) of the same samples investigated in our study identified four different sandstone types based on grain size, sorting, roundness, grain types, matrix amount, and cementation. However, the analysis was conducted solely using transmitted polarized light microscopy, without the inclusion of chemical measurements or

sufficient mineral phase determinations. Additionally, while the report provides written descriptions, it lacks supporting micrographs, making the findings harder to follow and visualize.

In contrast, our new approach emphasizes the alteration products of chemically and physically unstable mineral constituents—specifically feldspar and Fe-Ti-oxides—which are the primary contributors to the sandstone matrix. The matrix composition of sandstone can give valuable information about weathering and burial diagenesis conditions. Clay minerals (phyllosilicates) in the matrix are typical alteration products of feldspar and form as a result of erosion, transport, and deposition. Rock interaction with water commonly leads to chemical weathering and results in ion-enriched fluids, which remove the geochemically mobile elements, such as Ca, Na, and K (Chamley, 1989; Yuan et al., 2019). Moreover, rock-fluid interaction strongly affects the redox state of iron and, depending on the initial Fe-Ti-oxide assemblage, can lead to characteristic alteration series. For example, ilmenite ($FeTiO_3$) alteration typically progresses from pseudorutile ($Fe_2Ti_3O_9$) to rutile (TiO_2; Temple, 1966); however, anatase (TiO_2) may form as a minor component (Mücke and Bhadra Chaudhuri, 1991) or, in some cases, as the sole TiO_2 phase (Anand and Gilkes, 1984). By focusing on the Fe-Ti-oxide (namely ilmenite) and feldspar alteration products within Nubian sandstones, our investigation offers more detailed insights into the processes of erosion, transport, and deposition that formed the sandstone. Moreover, the pre-alteration Fe-Ti-oxide assemblage can be assessed, which sheds light on the potential geological provenance of the components that formed the Nubian sandstones after their deposition and cementation (e.g., Hou et al., 2021; Lindsley, 1991 and references therein).

We analyzed both the main mineral components and matrix constituents of the sampled sandstones, as well as the Fe-Ti-oxide assemblages using polarized light microscopy (transmitted and reflected), Raman spectroscopy, and scanning electron microscopy (SEM). These methods allow us to compare the genesis and depositional conditions of Nubian sandstones in greater detail, which we use to narrow down a common geological provenance for the components in the Temple A and quarry sandstones. From an archaeological perspective, we use the combination of Fe-Ti-oxide and feldspar alteration products and the sorting of the main rock-forming minerals to shed light on the sourcing practices employed by the builders of Temple A, which is significant because hieroglyphic texts reference "white stone" from Sai used in other New Kingdom temples in Nubia (Ullmann, 2020). Understanding these materials contributes to a deeper knowledge of Pharaonic building projects during the Egyptian colonial era in Nubia and their broader historical context.

1.1. Geology of Sai Island

Detailed geological field mapping of Sai Island has yet to be conducted. Its location between the 2nd and 3rd Nile cataracts resulted from a tectonic uplift zone trending east–west. The Nile subsequently incised into the uplifted Neoproterozoic crystalline basement and the overlying sedimentary cover (Geological Research Authority of Sudan, 2005; Thurmond et al., 2004). In the south-east and west of the island, metamorphic Precambrian rocks, including amphibolite and schist, occur together with quartzite, biotite gneiss, marble, and the sedimentary rock dolomite, which all dip around 30° towards the north-west and are commonly cross-cut by large quartz-veins (Draganits, 2014; Van Peer et al., 2003). In the northern and central part of the island overlying subhorizontal sediments occur, which comprise medium- to coarse-grained fluvial quartz sandstone, conglomerate and scarce siltstone, as well as silicified wood (Draganits, 2014). These sandstones are often referred to as "Nubian sandstone", however, this term is only vaguely defined and is argued to have no stratigraphic significance (Pomeyrol, 1968). Klemm and Klemm (2008, pp. 167–213) and Harrell (2024) provide detailed petrographic descriptions for some of the sandstones, and their associated quarries, used in ancient Egypt, including discussions of their functions and historical uses. Spence et al. (2009) describe a New Kingdom sandstone quarry at Sesebi, 80 km upriver from Sai Island. In contrast, other studies on Nubian sandstones primarily focus on their mechanical strength and physical properties (Elgendy et al., 2020; Nabawy et al., 2020, 2019, 2010). The present surface of Sai Island is formed of Pleistocene and Holocene Nile sediments that mostly consist of channel deposits of (sub-)rounded quartz, chert, and agate cobbles as well as floodplain sediments, which exhibit soil formation processes and associated calcrete (Draganits, 2014; Lewis et al., 2011) and are punctuated by small outcrops of quartzite and schist (Garcea and Hildebrand, 2009). In the central northeastern part of the island is the 75 m high Jebel Adou, an inselberg and a massive relict of the formation of Nubian sandstone, which penetrates the Nile sediment cover (Garcea and Hildebrand, 2009; Van Peer et al., 2003). The central southern part of the island has Nile gravel terraces, up to 15 m above the recent floodplain and composed of large quartz cobbles, which were used as raw material

Table 1
Summary of average (Ave), maximum (max), and minimum (min) grain sizes/long axes of the investigated Nubian sandstone samples with their average amount of matrix, sorting of grains, apparent bedding plane (BP, X if present), the occurrence of calcite (Cal, X if present) as well as their sampling source and the macroscopic Munsell rock color and applied analytical methods (OM = optical microscopy, Raman = Raman spectroscopy, SEM = scanning electron microscopy).

Sample	Grain size/Long Axes [µm]			Matrix Amount	Sorting	BP	Cal	Source	Munsell rock color	Analytical method
	Ave	Max	Min							
2	610	940	390	5–10 %	poor			quarry 1	Pinkish Gray (5YR 8/1)	OM, Raman
3	190	350	90	35 %	poor	X		quarry 2	Yellowish Gray (5Y 8/1)	OM, Raman
4	380	940	160	20–25 %	poor	X		quarry 2	Yellowish Gray (5Y 8/1)	OM, Raman
5	280	610	120	50 %	poor		X	quarry Adou	Reddish Brown (2.5YR 4/3)	OM, SEM, Raman
6	750	2640	310	20–35 %	poor		X	quarry 2	Yellowish Gray (5Y 8/1) to Pinkish Gray (5YR 8/1)	OM, Raman
7	170	270	110	50 %	poor		X	quarry Adou	Light Reddish Brown (2.5YR 6/4–7/4	OM, SEM, Raman
8	560	820	320	10–15 %	very poor	X		quarry 2	Pinkish Gray (5YR 8/1)	OM, SEM, Raman
9	360	790	190	35 %	poor		X	quarry Adou	Very pale orange (10YR 8/2)	OM, Raman
10	290	370	200	10–15 %	moderate			Temple A	Grayish Pink (5R 8/2)	OM, Raman
11	310	570	170	15 %	moderate			Temple A	Very Pale Orange (10YR 8/2)	OM, SEM, Raman
12	250	460	150	35–50 %	moderate			Temple A	Pinkish Gray (5YR 8/1)	OM, SEM, Raman
13	310	450	190	5–10 %	moderate			Temple A	Very pale orange (10YR 8/2)	OM, SEM, Raman
14	310	420	210	5–10 %	moderate	X		Temple A	Pinkish Gray (5YR 8/1)	OM, Raman
15	310	430	210	<5%	moderate	X		Temple A	Grayish Orange Pink (5YR 7/2)	OM, Raman
16	320	600	160	<5%	moderate			Temple A	Pinkish Gray (5YR 8/1)	OM, Raman
19	270	400	160	15–20 %	moderate			Temple A	Pinkish Gray (5YR 8/1)	OM, Raman
21	1150	2910	600	10–15 %	very poor		X	Temple A	Yellowish Gray (5Y 8/1) to Pinkish Gray (5YR 8/1)	OM, Raman
28	370	510	190	<5%	moderate			quarry 1	Grayish Red (5R 4/2)	OM, Raman
50	670	1330	350	5–10 %	poor			Temple A	Pinkish Gray (5YR 8/1)	OM, Raman

from the Paleolithic through to protohistoric times (Van Peer et al., 2003). The AcrossBorders project confirmed through on-site investigations that there was no quarrying at Jebel Adou during the Late Bronze Age (Budka, 2020, p. 44).

2. Methods and sampling

Fieldwork and sampling of sandstones from Temple A debris (Fig. 1b, c 20°44′13″N 30°19′55″E, samples 10–16, 19, 21, 50), as well as ancient quarry 1 (Fig. 1b, d; 20°44′20″N 30°19′56″E, samples 2, 28), quarry 2 (Fig. 1b, e; 20°44‘14“N 30°19‘55“E, samples 3, 4, 6, 8) and quarry Adou—adjacent to the village of Adou (Fig. 1b, f; 20°44’02”N 30°19’59”E, samples 5, 7, 9)—were conducted on Sai Island (Fig. 1a, b) in 2015 and 2016 (Budka, 2020, pp. 45-52). In total, 50 samples were collected non-destructively by gathering temple and quarry debris from the ground, rather than intrusively taking material directly from blocks used in the temple or the quarries themselves (Budka, 2020, p.43). Care was taken to ensure that the specimens were originally part of the temple or ancient quarries and that no decorations or inscriptions were present on the samples to avoid hindering conservation and research efforts. As shown in Fig. 1c, only the foundation and lower wall sections of the temple remain in situ while a large number of decorated blocks were found scattered throughout the site (Azim & Carlotti, 2012).

For the present study, uncovered and polished thin sections (≈25 μm) were prepared from 19 samples (Table 1) and investigated through optical microscopy (OM; Leica DM2700 P) using both transmitted and reflected polarized light. Photomicrographs were taken with a Leica MC170 HD camera and processed with the Leica Application Suite X 3.08.19082, which includes grain size measurements. Sorting describes the degree of uniformity in the sizes of clastic particles within a sample and is primarily controlled by the processes that transported and deposited the sediment. Grain angularity refers to the sharpness of the edges and corners on sediment grains. In this study, visual comparators were used to quantify grain sorting and angularity (Ulmer-Scholle et al., 2015; Janoo, 1998).

Six samples (Table 1) were studied with a Hitachi SU5000 SEM equipped with a field emission gun (NordlysNano), an energy-dispersive X-ray spectroscopy (EDS) detector (Oxford Instruments), a backscattered electron (BSE) detector, and a high-sensitivity electron backscatter diffraction detector (Oxford Instruments). SEM observations were conducted with a working distance of 10 mm and an accelerating voltage of 20 kV.

In situ micro-Raman spectroscopy was performed on all 19 samples with a HORIBA JOBIN YVON XploRa ONE system at the Mineralogical State Collection Munich (MSM; Staatliche Naturwissenschaftliche Sammlungen Bayerns, SNSB). The Raman spectrometer is equipped with a Peltier-cooled CCD detector and edge filters. A green 2ω-Nd:YAG laser (532 nm) was used together with an 1800 g/mm grate in an attenuated mode (10 % laser power) corresponding to max. 0.9 mW on the sample surface, which inhibits oxidation (Bauer et al., 2011), potentially leading to a false phase determination. Hole and slit diameters were 300 and 100 μm, respectively. A 100 × long working distance objective resulted in a 0.9 μm laser spot size. An integration time of 4 × 10 s was applied. The predominant 520 ± 1 cm^{-1} peak of a pure Si-wafer chip was used for wavelength calibration. The precision in Raman peak position is estimated to be ± 1.5 cm^{-1}.

Mineral phase determinations were performed using optical properties (polarization microscopy) and qualitative chemical compositions (SEM). For the investigation of the matrices and the Fe-Ti-oxides, phase determinations were determined and confirmed by structural investigations using Raman spectroscopy for the following minerals: anatase (Mazza et al., 2007; Ohsaka et al., 1978), hematite (Fe_2O_3; de Faria and Lopes, 2007; Wang et al., 2004), ilmenite (Dellefant et al., 2024; Wang et al., 2004), kaolinite ($Al_2Si_2O_5(OH)_4$; Wang et al., 2015), muscovite ($KAl_2(AlSi_3O_{10})(F,OH)_2$; McKeown et al., 1999), pseudorutile (Dellefant et al., 2024; Imperial et al., 2022), quartz (SiO_2; Trepmann et al., 2020), and rutile (Mazza et al., 2007).

The average macroscopic color of all samples was quantified with Munsell rock color chart (Deaton, 1987) using natural light.

3. Results

We begin with a general description of the petrography of the investigated Nubian sandstone samples (Figs. 2, 3), followed by an overview of the matrix-forming minerals (Figs. 4, 5). Finally, we document the Fe-Ti-oxide minerals present in the samples (Figs. 6, 7).

3.1. Main rock-forming constituents

The grains of all investigated sandstones (Fig. 2) with generally similar constituent compositions are quartz (90–95 vol%) and feldspar-group minerals (<10 vol%), which have (sub-)angular grains. If present, lithoclasts always represent < 5 vol%. The average grain sizes/long axes range from 190 μm to 1150 μm (Table 1). Throughout all samples, the amount of matrix varies from < 5 % to 50 %. The compositional dominance of quartz in combination with a matrix amount below 15 %, defines samples 2, 8, 10, 13, 14, 15, 16, 28 and 50 as quartz arenites, whereas samples 3, 4, 5, 6, 7, 9, 11, 12, and 19 have an amount of matrix ranging from 15 % to 50 % and are, therefore, quartz wackes, which have a comparably lower textural maturity (Dott, 1964; Pettijohn et al., 1987). A bedding plane can be observed in samples 3, 4, 8, 14, and 15 (Fig. 2a; Table 1). Feldspars are commonly rich in K with K/Na ratios, varying from 0.9 to 1 as indicated by EDS measurements (Fig. 2e-h) with only minor occurrences of plagioclase ($Na_{1-x}Ca_xAl_{1+x}Si_{3-x}O_8$).

Samples from the ancient quarries (Fig. 1b, d-f; samples 2–9; Table 1) have poor to very poor sorting (except sample 28 with moderate sorting), where average grain sizes range from 190 μm to 750 μm (Fig. 2c). Matrix amounts are on average larger than 15 %, which classifies the samples mostly as quartz wacke (67 % of quarry samples; Table 1). The Munsell rock colors (Table 1) range from pinkish/yellowish gray to very pale orange (5YR 8/1, 5Y 8/1, 10YR 8/2) to (light) reddish brown (2.5YR 6/4–7/4, 2.5YR 4/3) and grayish red (5R 4/2).

In contrast, samples from Temple A (Fig. 1b, c; samples 10–16; Table 1) generally have moderate sorting with average grain sizes typically in the 250 μm to 310 μm range (Fig. 2d; Table 1). However, sample 21 has very poor sorting with an 1150 μm average grain size (Fig. 3d; Table 1) and sample 50 poor sorting with a 670 μm average grain size. Matrix amounts are on average lower than 15 %, which classifies the samples mostly as quartz arenites (70 % of temple samples; Table 1). The Munsell rock colors (Table 1) range from pinkish/yellowish gray (5YR 8/1, 5Y 8/1), very pale orange (10YR 8/2) to grayish (orange) pink (5R 8/2, 5YR 7/2) and appear generally lighter in color compared to the ancient quarry samples.

All samples have ≈30 % of quartz grains with undulose extinction (Fig. 3a, b), characteristic of intracrystalline plastic deformation (Blenkinsop, 2002). Calcite ($CaCO_3$) within vesicles or as part of the matrix occurs only in samples with (very) poor sorting (samples 5–7, 9, 21; Fig. 3b; Table 1). A rim of μm-thick illite group mineral(s) ($K_{1.5-1.0}Al_4[Si_{6.5-7.0}Al_{1.5-1.0}O_{20}](OH)_4$; Fig. 3c) around quartz and feldspar occurs predominantly in Temple A samples (samples 11, 13, 14, 15, 19, 50) but also in sample 2 from quarry 1. Although having similar constituents to the rest of the sample set, sample 21 has an average grain size of 1150 μm with about 60 % of rock-forming quartz grains displaying deformation features, such as undulose extinction and recrystallization (Fig. 3d). In all samples, accessory phases, such as phyllosilicates, with lengths of hundreds of μm, including muscovite and biotite (biotite, $K(Mg,Fe,Mn)_3[(OH,F)_2|(Al,Fe,Ti)Si_3O_{10}]$; Fig. 2d) occur.

3.2. Matrix-composing minerals

Across all investigated samples (except sample 21), 80–95 % of the

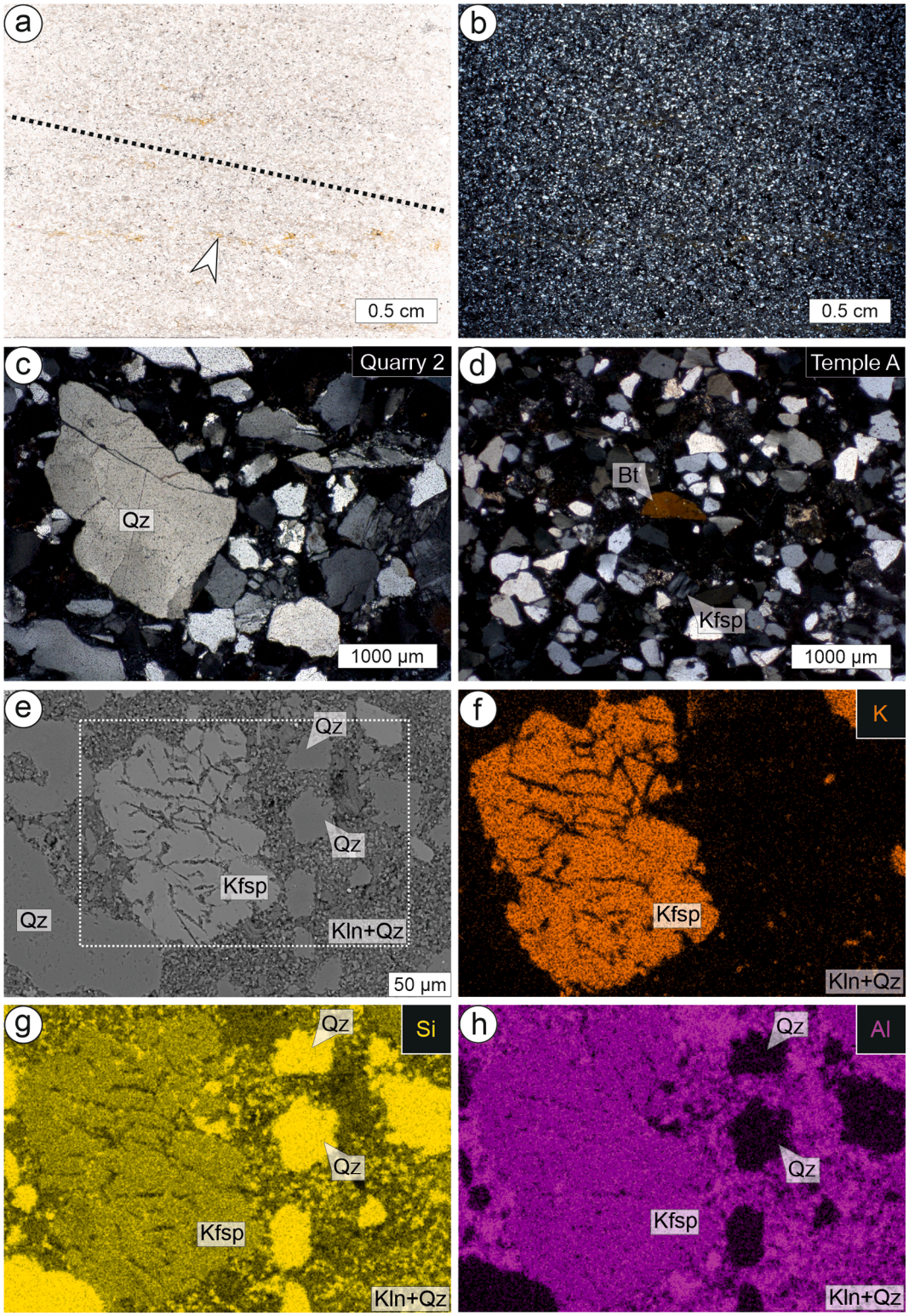

Fig. 2. Overview of Nubian sandstone samples and their rock-forming minerals. **a, b)** Polarized light micrographs of sandstone fabric with the dashed line indicating the orientation of the bedding plane and the white arrow pointing to yellow-coloring Fe-hydroxides; sample 3; (b) taken with crossed polarizers. Sandstones from quarries commonly have **c)** (very) poor sorting (sample 6), whereas samples from Temple A generally have **d)** moderate sorting (sample 15) of the main constituent quartz (Qz) and the minor constituents K-feldspar (Kfsp) and phyllosilicates, such as biotite (Bt). **e)** BSE image of fractured K-feldspar (Kfsp) and adjacent quartz (Qz) within a matrix consisting of kaolinite (Kln) and quartz. The white dashed rectangle indicates the location of the chemical maps shown in (f-h); sample 7. Chemical distribution maps of **f)** K, **g)** Si, and **h)** Al.

matrix is composed of an assemblage of mostly few-µm-sized kaolinite and quartz (Fig. 4a, b). Minor constituents are illite group mineral(s) (<5–20 %; Fig. 4d-f), hematite, and Fe-hydroxides ($FeO(OH)\cdot nH_2O$) (Fig. 5). However, the proportions of these components vary across the thin sections as does the amount of matrix (5–50 %; Table 1). In contrast, the matrix of sample 21 mostly comprises few-µm-sized quartz. Calcite

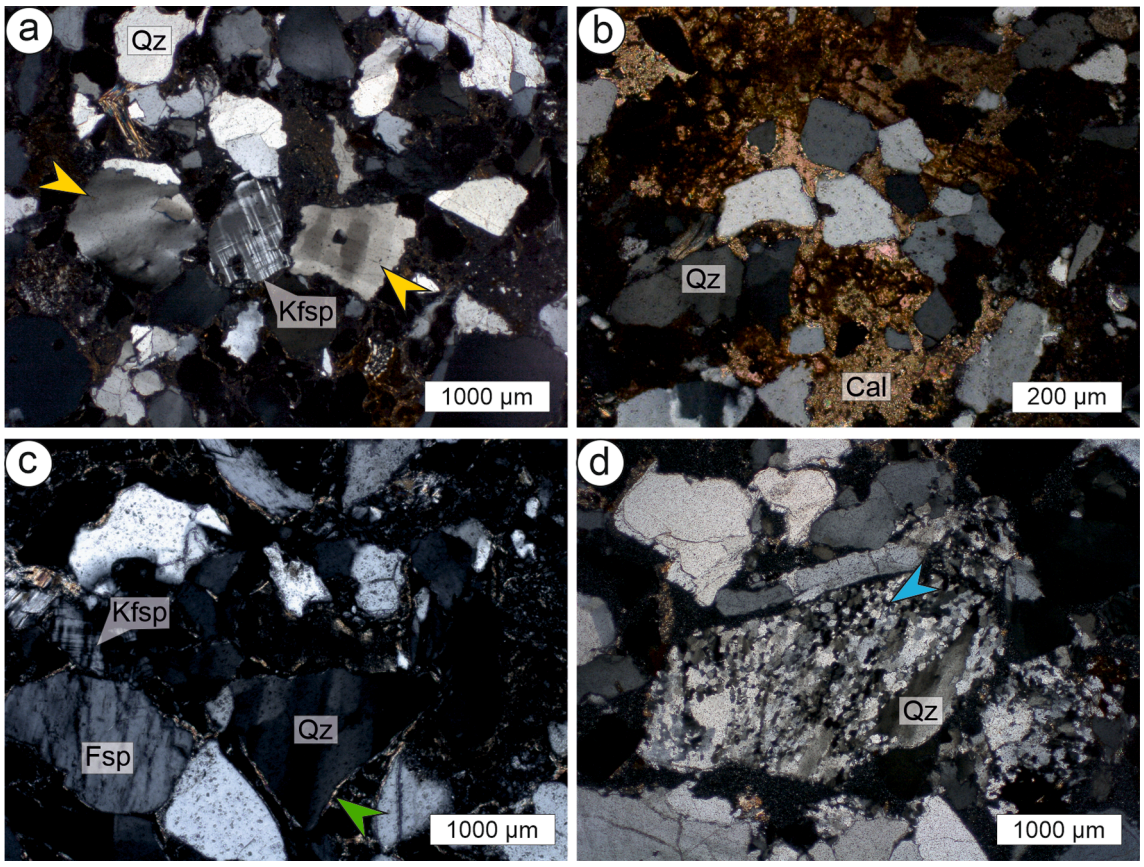

Fig. 3. a) Quartz (Qz) locally has undulose extinction (yellow arrows) and K-feldspar (Kfsp) has grid-like twins (sample 50). **b)** Calcite (Cal) can occur as a matrix constituent; sample 9. **c)** Quartz (Qz) with undulose extinction with a rim of phyllosilicates (green arrow) adjacent to feldspar (fsp) and K-feldspar (Kfsp); sample 11. **d)** Quartz (Qz), which is almost completely recrystallized (blue arrow) indicating a metamorphic origin; sample 21.

occupying former vesicles occurs as minor phase (Table 1), whereas in sample 9 calcite makes up ≈10 % of the overall matrix (Fig. 3b, Table 1).

Kaolinite can also occur as a few hundred of µm-long grains within the matrix (Fig. 4c). Nevertheless, Raman spectra locally have additional peaks at 1046, 1115, and 1404 cm^{-1}, which might be attributed to muscovite (McKeown et al. 1999). Illite group mineral(s) have comparably higher interference colors than kaolinite and quartz (Fig. 4a) and were confirmed with EDS measurements, where K/Al ratios range from 0.2 to 0.4, Si/Al ratios from 0.6 to 0.7, (Mg + Fe)/Si ratios from 0.06 to 0.14, and Mg/Fe ratios from 0.4 to 1.3 (Deer et al., 2013 and references therein). No Raman spectra of illite could be acquired with the 532, 638, and 785 cm^{-1} excitation laser wavelength due to a low signal-to-noise ratio and a high fluorescence background.

Fe-hydroxides (Fig. 2a) and hematite (Fig. 5) are mostly present as few-µm-sized grains within the matrix. Nevertheless, hematite also occurs within polycrystalline aggregates, which have a diameter of hundreds of µm (Fig. 5a). Moreover, hematite commonly occurs as few tens of µm-sized aggregates along grain boundaries of the main rock-forming minerals quartz and feldspar (Fig. 5a). Rarely, hematite could be observed within calcite aggregates, precipitated in vesicles of the quartz arenites (Fig. 5b, c).

3.3. Fe-Ti-oxide minerals

Fe-Ti-oxide minerals occur from > 1 % to 3 % throughout the samples (Table 2). Ilmenite could only locally be verified (samples 3 and 4) in the center of Fe-Ti-oxide aggregates rimmed by rutile, which have lengths of about hundred µm (Fig. 6a, b, Fig. 7a). Due to alteration, ilmenite Raman spectra have a broader band at 291 cm^{-1} which might be associated with hematite (Fig. 7a; Wang et al., 2004), whereas additional peaks at 438 cm^{-1} and 615 cm^{-1} might be the main peaks of rutile (Fig. 7a, d; Mazza et al., 2007). Pseudorutile (Fig. 6c), having a length of about hundred µm, commonly occurs locally associated with rutile (Fig. 7c, d). The very broad and overlapping Raman bands of pseudorutile (Fig. 7b-d) indicate a rather amorphous structure (Dellefant et al., 2024; Imperial et al., 2022). With an increasing degree of alteration (Temple, 1966), the Raman spectra of pseudorutile show an increase in relative intensity of a Raman peak at ≈455 cm^{-1} corresponding to rutile (Fig. 7b-d). Although consisting both of TiO_2, the final ilmenite alteration products rutile (Fig. 7e) and anatase have characteristic Raman spectra (Fig. 7f). Anatase can either occur within altered ilmenite grains, as a honeycomb-like structure (Fig. 6d) with a length of about 100 µm, or as µm- to tens of µm-sized grains within reaction aggregates of about hundred µm alongside µm-sized rutile (Fig. 6e, f). Rutile (Fig. 7e) occurs as µm-sized grains within aggregates together with anatase (Fig. 6e, f) forming a rim, a few µm thick, around altered ilmenite (Fig. 6a, b), or rarely as monocrystalline ≈60 µm long grain (Fig. 6e, f). Rarely, hematite occurs as a monocrystalline phase with a length of ≈60 µm.

4. Discussion

We integrate mineralogical, petrographical, and geochemical analyses of Nubian sandstone from Temple A and associated quarries on Sai Island to evaluate both their geological origins and the alterations these rocks experienced. The discussion summarizes the findings from our analyses of the main rock-forming grains, matrix-forming minerals, and Fe-Ti-oxide assemblages before considering the wider implications of the study in relation to Temple A. This approach reveals strong mineralogical and petrographical similarities between all investigated

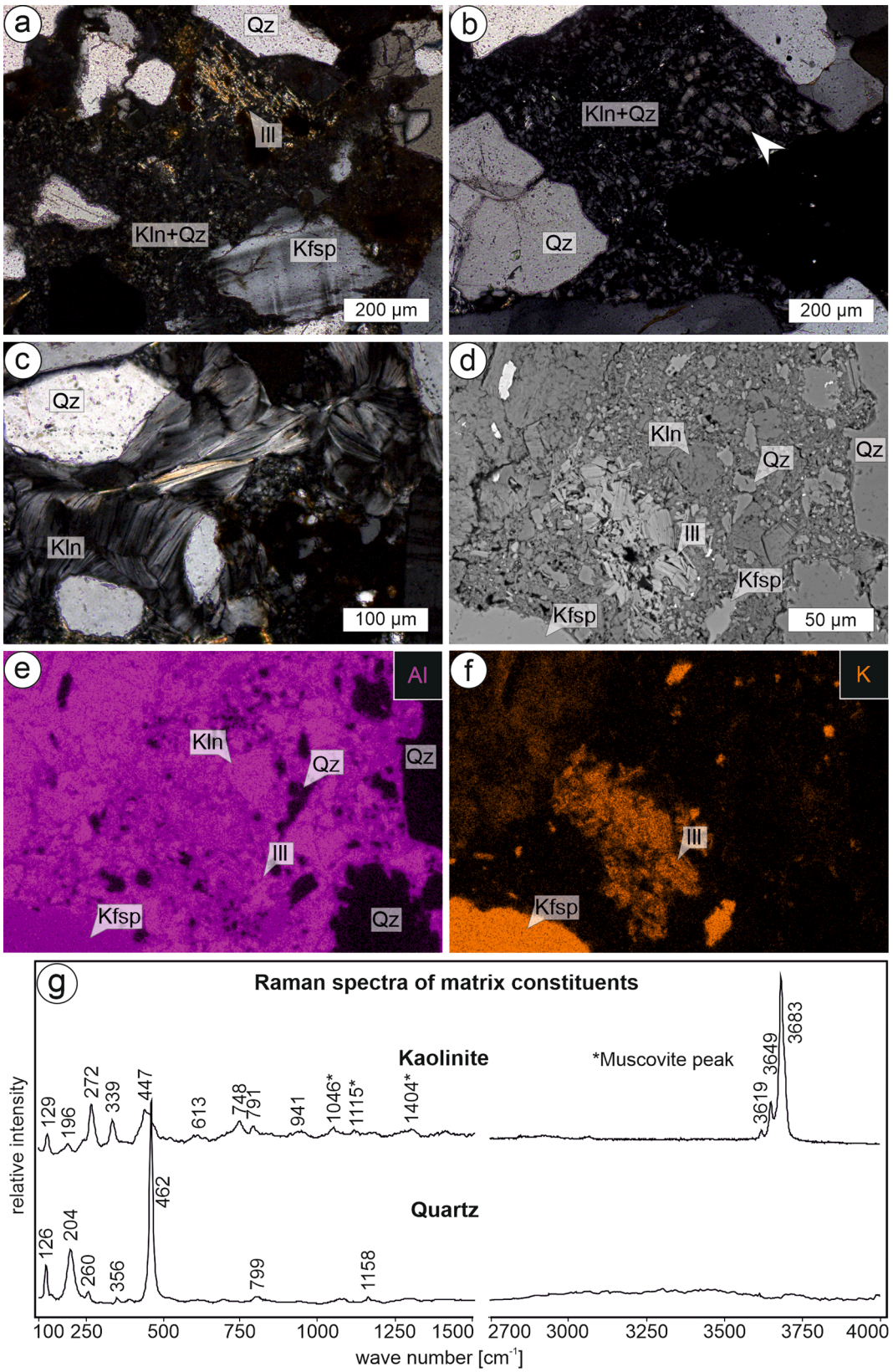

Fig. 4. Matrix-composing silicates cementing the quartz (Qz) and K-feldspar (Kfsp) grains in the Nubian sandstones. **a)** Illite (Ill) together with kaolinite (Kln) and quartz; sample 13. Kaolinite can occur **b)** in sizes from a few µm up to tens of µm-long vermicular aggregates (white arrow; sample 2) or **c)** as 100 s of µm-sized grains (sample 11). (a-c) polarized light micrographs with crossed polarizers. **d)** BSE image and chemical distribution maps of **e)** Al and **f)** K depicting illite (Ill), kaolinite (Kln), and quartz within the matrix adjacent to quartz and K-feldspar grains; sample 12. **g)** Raman spectra of kaolinite and quartz within the matrix; sample 11 and 21, respectively.

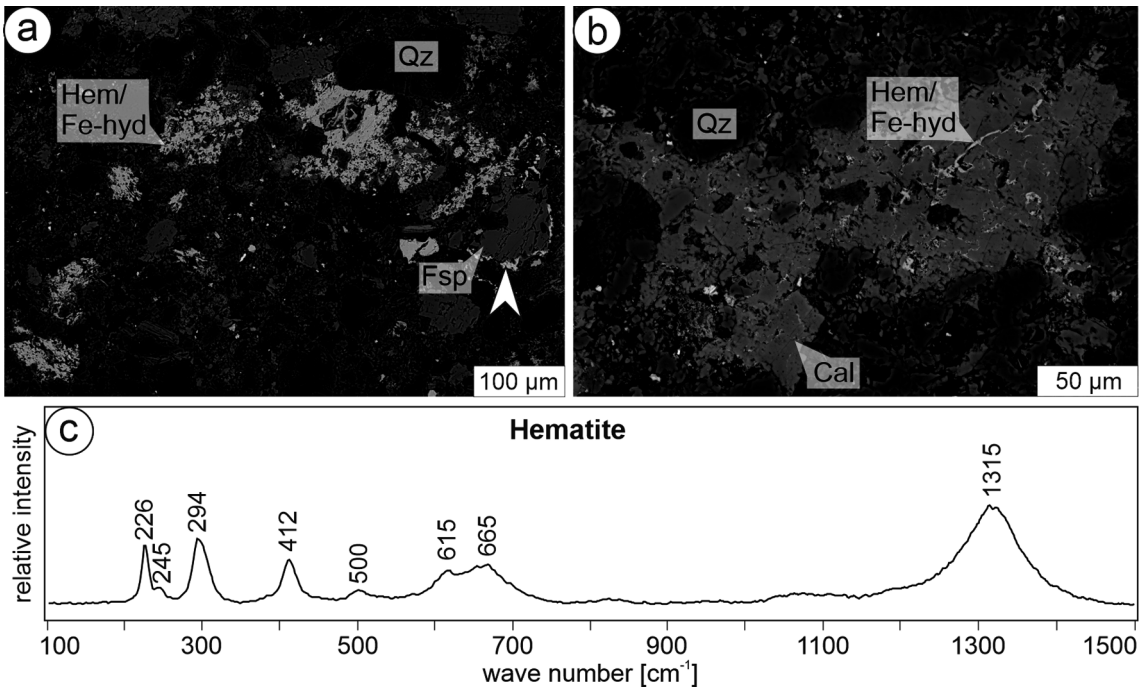

Fig. 5. Hematite (Hem) and Fe-hydroxides (Fe-hyd), which can occur as **a)** polycrystalline aggregates, along grain boundaries (white arrow) of quartz (Qz; dark grey) and feldspar (Fsp; light grey) grains or **b)** within calcite (Cal), sample 5. **c)** Raman spectrum of hematite; sample 50.

samples, supporting the conclusion that they likely derive from a common geological source and the same stratigraphic unit on Sai Island.

4.1. Main rock-forming constituents

Mineralogically, the grains of the investigated Nubian sandstones are dominated by quartz (>90 %), feldspar (<10 vol%), and minor lithoclasts (<5 vol%). The compositional dominance of quartz grains across all investigated samples indicates mineralogic maturity. Samples can be defined as quartz wackes and quartz arenites dependent on their matrix amount (Table1; Dott, 1964; Pettijohn et al., 1987). However, the petrographic analysis was conducted using polarization microscopy on thin sections and is, therefore, limited to a relatively small sample volume (approx. 2.5 cm × 1 cm × 25 µm), which could also represent heterogeneities within stratigraphic units that are more homogeneous at a larger scale.

The majority of the temple sandstones have moderate sorting, similar grain sizes (250 to 310 µm; Fig. 2d; Table 1) and appear only in light Munsell rock colors, which generally correlates with a lower amount of matrix and classification as quartz arenites (Table 1). In comparison, most of the investigated sandstones from ancient quarries display (very) poor sorting, associated with a stronger scattering in grain sizes (190 to 750 µm) and locally darker Munsell rock colors (Fig. 2c; Table 1), correlated with higher average amounts of matrix and quartz wacke classifications. Generally, sorting relates to a decrease in porosity and an interconnected pore network (Rogers and Head, 1961). We propose that fluid percolation was facilitated in the quarry samples, resulting in the higher amount of matrix compared to the temple samples. This resulted in the formation of hematite and Fe-hydroxides, leading to a darker macroscopic appearance. We can exclude recent weathering effects as the cause of macroscopic color differences between quarry and temple samples because all samples, and their respective locations, experienced the same climatic conditions and there was no difference in sampling.

The main grain constituents of the sandstone, quartz and feldspar, suggest an igneous origin. However, about 30 % of quartz grains show undulatory extinction (Fig. 3a, c) and, as such, deformation which could indicate an additional metamorphic source (Basu et al., 1975). In all samples, plagioclase is either absent or occurs as a minor phase in the feldspar-group (Fig. 2e-h). Based on an investigation of the Panola granite, White et al. (2001) reported that feldspar weathering is mainly controlled by chemical compositions and related solubilities. Their thermodynamic calculations predict that the endmember albite ($NaAlSi_3O_8$) of Na-plagioclase is about 400 times more soluble than K-feldspar ($KAlSi_3O_8$) in meteoritic water. Therefore, the scarce occurrence of plagioclase across all of our samples, in combination with their textural and compositional maturity could be the result of progressive feldspar alteration before or during deposition, potentially in combination with a humid paleoclimate.

4.2. Matrix-forming minerals and implications for burial diagenesis conditions

The matrix of all temple and quarry sandstones (except sample 21) consists of few-µm-sized to tens-of-µm-sized kaolinite and quartz (Fig. 2e-h, Fig. 4) with additional Raman peaks, which might be attributed to muscovite (Fig. 4g) and minor occurrences of few-µm-sized illite (Fig. 3c, Fig. 4a, d, f). Kaolinite formation is generally associated with feldspar weathering in early diagenesis conditions, driven by the interaction with, for example, feldspar and meteoritic water (Dill, 2016 and references therein; Huertas et al., 1999; Lanson et al., 2002). The reactions can be expressed as the following for the K-endmember of alkali-feldspar [$(Na,K)AlSi_3O_8$; Equation (1) and the Na-endmember of plagioclase Equation (2)]:

$$2KAlSi_3O_8 + 2H^+ + H_2O \rightarrow Al_2Si_2O_5(OH)_4 + 2\,K^+ + 4SiO_{2(aq)} \quad (1)$$

$$2NaAlSi_3O_8 + 2H^+ + H_2O \rightarrow Al_2Si_2O_5(OH)_4 + 2Na^+ + 4SiO_{2(aq)} \quad (2)$$

Therefore, the precursor of kaolinite in our samples was either i) plagioclase, which almost completely transformed, or ii) a combination of K-feldspar and plagioclase, where the latter was preferentially transformed; either of which could explain the minor occurrence of plagioclase. In both cases, the feldspar likely interacted with an acidic solution as similarly reported from immature K-feldspar-rich sandstones by Shah and Bandyopadhyay (2005) for the Parsora sandstones in India.

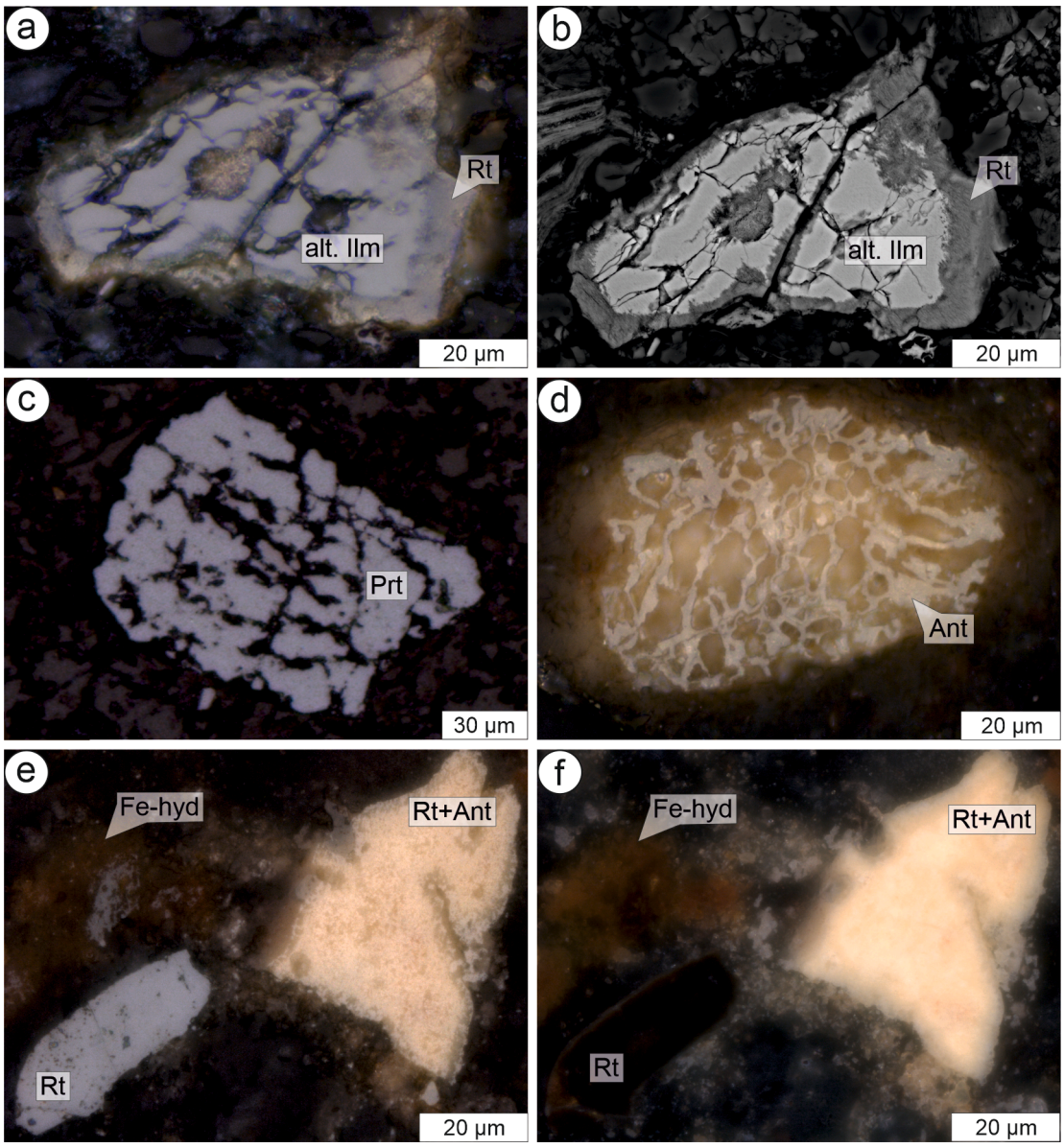

Fig. 6. Fe-Ti-oxides within Nubian sandstones. **a, b)** Altered ilmenite (alt. Ilm) with a rim of rutile (Rt). **c)** Pseudorutile (Prt). **d)** Anatase (Ant). (a-d) Sample 5. **e, f)** Polycrystalline aggregate of rutile and anatase (Rt+Ant) adjacent to monocrystalline rutile (Rt) and Fe-hydroxides (Fe-hyd); sample 7. (a, d, e) reflected polarized light micrographs as well as (f) with crossed polarizers; (b) BSE image.

Generally, the formation of kaolinite from feldspar is thought to produce a stress-induced dissolution of feldspar due to volumetric constraints (Merino et al., 1993). The occurrence of few-µm-sized (Fig. 4a, b) and hundreds-of-µm-sized kaolinite grains (Fig. 4c) could indicate a multi-stage matrix formation process with kaolinite first forming and then growing locally. Kaolinite is considered to remain stable in moderate burial depths and at temperatures ranging from 80 °C to 160 °C (Cuadros et al., 2014 and references therein). That said, kaolinite might be metastable with respect to dickite, which forms at higher temperatures, from at least 350 °C (Zotov et al., 1998). Chemical EDS analysis quantified an absence of Na within the matrix constituents where only minor K-bearing illite group phase(s) are present (Fig. 2e-h, Fig. 4d-f). The illite group is common in sedimentary rocks and can be formed from a variety of precursor phases, such as feldspar (Huang et al., 1986) and kaolinite (Berger et al., 1997; Sass et al., 1987). Kaolinite usually predates illite (Lanson et al., 2002 and references therein) and, as such, might have been the precursor in our samples, as also documented for shallow-buried sandstone units from the Norwegian continental shelf (Ehrenberg et al., 1993). However, clay minerals can transform into other clay species with changes in climatic or burial conditions and an increase in weathering (Hong et al., 2015; Lanson et al., 2002; Singer, 1980). Illitization of kaolinite is more likely in elevated K^+/H^+ environments, where K^+ can migrate when temperatures exceed 120 °C often in moderate- to deep-burial diagenesis (Bentabol et al., 2003; Ehrenberg, 1989; Lanson et al., 2002 and references therein). Calcite occurs locally within vesicles (Fig. 3b) intermingled with µm-sized hematite and Fe-hydroxides (Fig. 5b), which also occur locally along grain boundaries of rock-forming minerals (Fig. 5a). Therefore, calcite and hematite/Fe-hydroxides likely formed simultaneously and precipitated together from a fluid.

Due to the chemical similarities of the sample matrices (Fig. 4), despite the varying quantities of matrix (5–50 %; Table 1), no systematic differentiation can be identified by comparing sandstones from Temple A with ancient quarries 1 and 2 or quarry Adou, except for sample 21 from Temple A, which has a matrix dominated only by few-µm-sized quartz.

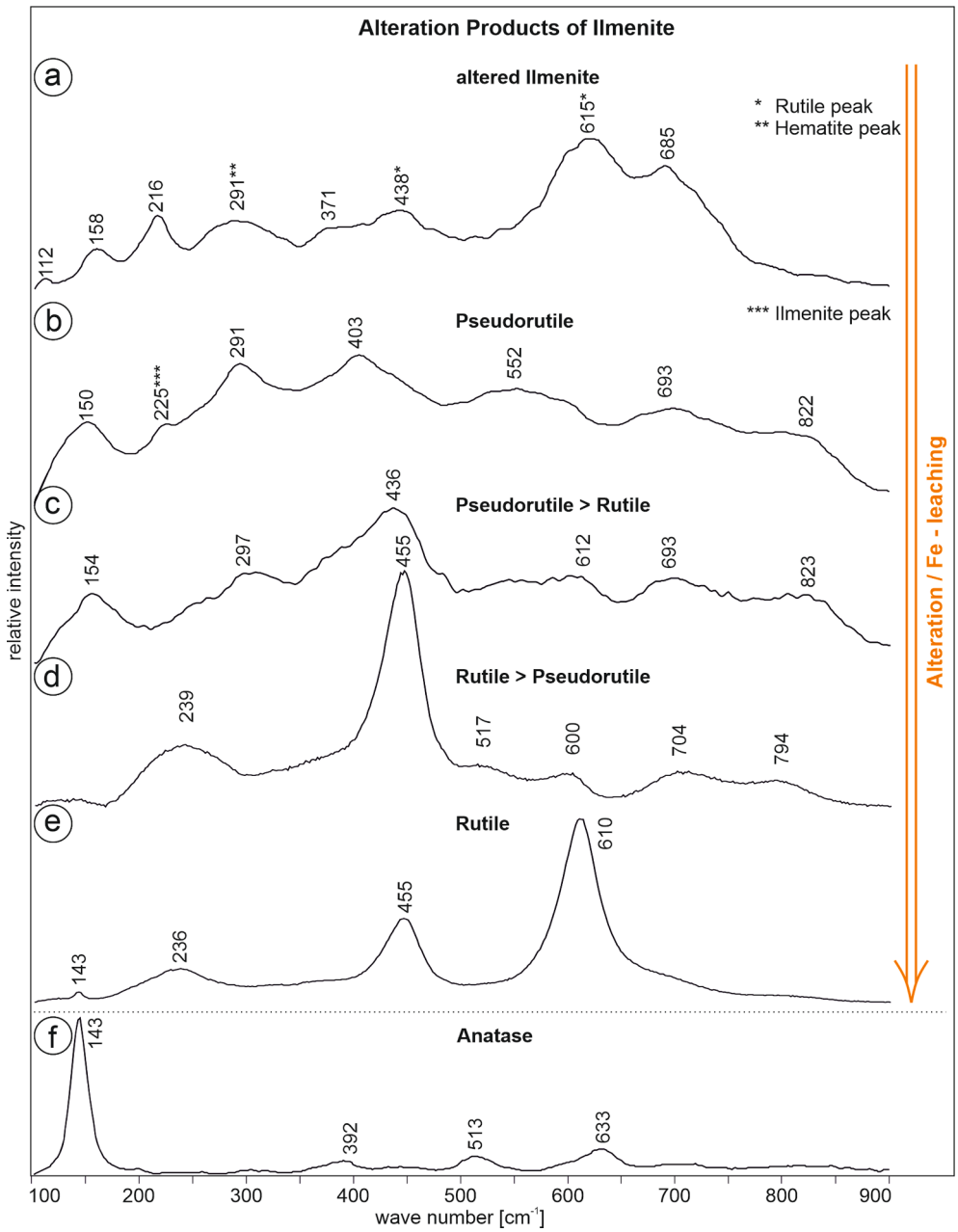

Fig. 7. Ilmenite alteration products and evolution of respective Raman spectra with subsequent Fe-leaching based on Temple (1966). Increasing alteration forms **a)** altered ilmenite (sample 5), **b)** pseudorutile (sample 5), **c)** pseudorutile and minor rutile (sample 4), **d)** rutile and minor pseudorutile (sample 4), and **e)** rutile (sample 2). Although **f)** anatase forms as an alteration product of ilmenite, its relative time of generation in the alteration series cannot be ascertained.

4.3. Ilmenite alteration products

Altered ilmenite (Fig. 6a, b, Fig. 7a), pseudorutile (Fig. 6c, Fig. 7b-d), rutile (Fig. 6a, b, e, f, Fig. 7e), and anatase (Fig. 6d-f, Fig. 7f), occur from > 1 % to 3 % throughout the samples (Table 2) and are products of ilmenite alteration (Fig. 7) together with hematite (Fig. 5) and Fe-hydroxides (Fig. 2a, Fig. 5a, b). During ilmenite alteration toward rutile, pseudorutile forms as a transitional phase [Equation (3); Temple, 1966; Teufer and Temple, 1966] below 700 °C and under high oxygen fugacity conditions, which involves oxidation of Fe^{2+} to Fe^{3+} (Gupta et al., 1991).

$$3Fe^{2+}TiO_3 \rightarrow Fe_2^{3+}Ti_3O_9 + Fe^{3+} \quad (3)$$

This process starts along grain boundaries and/or structural discontinuities within the grain (Grey and Reid, 1975; Temple, 1966) utilizing a leaching agent, such as water (Mücke and Bhadra Chaudhuri, 1991). Upon continuous alteration and Fe-leaching, rutile and anatase (Equation (4) form as final products (Temple, 1966) together with hematite [Equation (5) and Fe-hydroxides Equation (6)].

$$Fe_2^{3+}Ti_3O_9 \rightarrow 3TiO_2 + 2Fe^{3+} \quad (4)$$

$$4Fe^{3+} + 3O_2 \rightarrow 2Fe_2O_3 \quad (5)$$

$$Fe^{3+} + (n+1)H_2O \rightarrow FeO(OH)\cdot nH_2O \quad (6)$$

Anatase occurs locally in our samples as a honeycomb-like structure (Fig. 6d) with a length of about 100 μm, which could be a result of

Table 2
Occurrences and distributions of Fe-Ti-oxide minerals (Rt = rutile; Ant = anatase; Prt = pseudorutile; alt. Ilm = altered ilmenite) within Nubian sandstones.

Sample	Source	Fe-Ti-oxide [vol. %]	Rt	Ant	Prt	alt. Ilm
			[%]			
2	quarry 1	>1	100			
3	quarry 2	>1	60	10	10	20
4	quarry 2	>1	50	20	30	
5	quarry Adou	3	30		70	
6	quarry 2	1–2	50	10	40	
7	quarry Adou	1–2	50		50	
8	quarry 2	>1	100			
9	quarry Adou	1–2	20		80	
10	Temple A	1–2	40	10	50	
11	Temple A	1–2	60		40	
12	Temple A	3	70	10	20	
13	Temple A	1–2	30		40	30
14	Temple A	1–2	20		80	
15	Temple A	1–2	20	10	70	
16	Temple A	1–2	20	10	70	
19	Temple A	1–2	70		30	
21	Temple A	>1			100	
28	quarry 1	3	100			
50	Temple A	>1	60		40	

leaching where iron was completely removed from the ilmenite precursor and the conditions where not suitable for a transformation from anatase to rutile. In contrast, the occurrence of μm-sized rutile and anatase in about 100 μm sized aggregates indicates (Fig. 6e-f) that anatase–rutile transformation conditions are heterogeneously distributed in accordance with the occurrence of only rutile as a rim around altered ilmenite (Fig. 6a, b).

Within alteration products, we found no lamellae and only rarely exsolution structures (Fig. 6d), which chemically could, in theory, be attributed to Ti-magnetite alteration but has not been reported from geologic samples to our knowledge. Both hematite and rutile grains can occur as a monocrystalline phase with lengths of ≈60 μm (Fig. 6e, f). Due to their size, their occurrence as single monocrystalline grains, they are likely no ilmenite alteration products. Therefore, we conclude that, initially, only ilmenite with minor occurrences of hematite and rutile were present as a group of the Fe-Ti-oxides in the sediment.

4.4. Implications for provenance analysis and sourcing practices of the ancient builders of Temple A

The sandstone grains mostly originate from a magmatic system based on the dominance of the rock-forming mineral grains quartz and feldspar (Fig. 2a-d), with about 30 % of quartz grains showing undulose extinction of quartz as a result of deformation (Fig. 3a, c). Based on the investigation of the Fe-Ti-oxide assemblage present in all of the samples analyzed (Figs. 5-7), we conclude that in both the temple and quarry samples, only ilmenite, rutile, and hematite were present prior to alteration as a group of the Fe-Ti-oxides. Generally, Fe-Ti-oxides in magmatic systems are considered to represent the late-evolution stage temperature and oxygen fugacity conditions of their reservoirs at depth (Hou et al., 2021). The evolution of Fe-Ti-oxide minerals within magma chambers can be considered as a parallel system to silicates. Therefore, the investigation of the Fe-Ti-oxides in the Nubian sandstones can give insights into the provenance of the sediment's components. Experimental research on oxide minerals has been carried out to establish calibrations for different thermodynamic systems (Ghiorso and Sack, 1991; Lattard et al., 2005; Lattard and Partzsch, 2001; Lindsley, 1991 and references therein; Sauerzapf et al., 2008). Ilmenite with minor hematite and rutile can thermodynamically be attributed to a narrow temperature and pressure window (e.g., T≈600 °C, P = 1–2 kbar; Lindsley, 1991 and references therein), which likely represents the order of magnitude of the late-evolution stage of magmatic reservoirs at depth (Hou et al., 2021), from which the grains of the Nubian sandstone samples derive. However, it is possible that additional magmatic sources with similar late-stage evolution temperatures and oxygen fugacity conditions contributed to the sediment constituents.

The temple sandstones mostly have moderate sorting and similar grain sizes (250–310 μm; Fig. 2d; Table 1) with the occurrence of mostly light Munsell rock colors. In comparison, the majority of the investigated ancient quarries display (very) poor sorting, stronger scattering in grain sizes (190–750 μm), and generally darker Munsell rock colors (Fig. 2c; Table 1). The assemblages of the main constituents (Figs. 2, 3; Table 1), the matrices (Figs. 4, 5), and the ilmenite alteration products (Figs. 6, 7) are very similar across the investigated Nubian sandstones, except for sample 21 as discussed above. Therefore, we conclude that all investigated samples (except sample 21) might be from the same, or very similar stratigraphic units, on Sai Island. Further interpretation requires a detailed geological study of the stratigraphy of Sai Island, which has not been conducted to our knowledge. Due to the different matrix composition of sample 21 (quartz-dominated) as well as recrystallized quartz indicating a metamorphic overprint (Fig. 3d), it could originate from a different stratigraphic unit or from outside Sai Island. We suggest that the differences between the temple samples and those from the quarries—in terms of grain size, sorting, and Munsell rock color—are the result of selective quarrying by masons from the same stratigraphic unit. The remaining Nubian sandstone in the ancient quarries is, therefore, likely residual material, which was not considered suitable as building material. We propose that ancient builders carefully selected sandstone blocks to ensure the noticeable similarity in appearance between the different building blocks used in Temple A. This might have been achieved by using a reference sample of temple-quality Nubian sandstone. However, with our data set, allocating the provenance of temple sandstones to distinct quarries on Sai Island does not seem feasible. While our results suggest a common provenance for the investigated samples, further sampling from all ancient quarries on Sai Island is necessary to conclusively map the full range of building stone sources for Temple A.

Regarding the sourcing practices of the ancient builders of Temple A, Dietrich and Rosemarie Klemm suggested in 2016, based on petrographic analyses and observations of the chisel marks, that the builders of Temple A on Sai Island made a clear choice between the aesthetic quality and durability of the sandstone available on the island (Budka, 2024, p. 28). Aesthetic-qualities were noticeably prioritized for temple buildings, and this might have also influenced the choice of sandstone from Sai in other building projects in Nubia, as suggested by textual sources. Specifically, the contemporary toponym for Sai, *Š3ᶜ.t*, is repeated five times in the inscriptions of the 18th Dynasty temple of Kumma (Semna East) as a source of building material for the temple (Ullmann, 2020). Kumma is located 112 km north of Sai, and the Dal cataract and the Batn el-Hagar represent significant natural barriers between the two sites. For this reason, and because of the logistics of stone transport, Didier Devauchelle and Florence Doyen (2009, p. 36) have expressed doubts that Sai Island could be a source for the building material used at Kumma. Since a building inscription in Kumma mentions stone from *T3-Stj* for 'Nubia' and not from *Š3ᶜ.t* for 'Sai', Devauchelle and Doyen suggest that in this context both toponyms refer to a larger metaphorical region. Although this remains a possibility, Martina Ullmann has shown that there are more arguments in favor of taking the reference to *Š3ᶜ.t* (as part of *T3-Stj*) more literally (Ullmann, 2020, pp. 56-58). She took into account the geology and landscape of the 2nd cataract and the Batn el-Hagar region, where no sandstone formations are found. The temple of Kumma was, therefore, necessarily built with stones brought from elsewhere — be it from the north, the region of Wadi Halfa, or from the south, the region of Sai. Ullmann (2020, p. 57) pointed out that transport northwards following the Nile current would be easier than shipping upstream, which makes it more likely that the Kumma blocks originated from Sai Island. Overall, this would correlate with our new findings on the provenance of the Temple A blocks from Sai Island.

5. Conclusions

We investigated the main rock-forming grains as well as ilmenite alterations and matrix compositions of Nubian sandstones from Sai Island (northern Sudan) by analyzing and comparing ten Temple A samples and nine ancient quarry samples:

- Nubian sandstones from both Temple A and ancient quarries on Sai Island exhibit highly similar mineralogical and petrographic characteristics, dominated by quartz (>90 %), minor feldspar (<10 %), and rare lithoclasts (<5%) grains.
- Alteration products of ilmenite (pseudorutile, rutile, anatase) and feldspar (matrix: kaolinite, illite) are present in all samples, indicating comparable weathering, diagenetic, and burial histories across temple and quarry sandstones.
- The Fe-Ti-oxide assemblage before alteration was ilmenite with minor rutile and hematite in all samples which points, together with the highly similar whole rock mineralogical and petrographic characteristics, to a late-stage magmatic source with similar temperature, pressure, and oxygen fugacity conditions, supporting the interpretation of a common provenance for the sandstones analyzed.
- Temple A sandstones are characterized by moderate sorting, smaller and more uniform grain sizes (250–310 μm), and lighter Munsell colors, in contrast to quarry samples, which are more poorly sorted, coarser, and darker; this pattern suggests intentional selection by ancient stonemasons for aesthetic and material consistency.
- Despite detailed mineralogical analysis (polarized light microscopy, SEM, Raman spectroscopy), the homogeneity of the sandstones precludes precise attribution of Temple A blocks to specific quarries on Sai Island. However, it is very likely that all of the investigated samples derive from the same stratigraphic unit.

6. Outlook

A petrographic examination of samples from the temple of Kumma, and ideally from the neighboring contemporaneous temple at Semna, along with a comparative analysis of temple samples from Sai Island, could provide the solution to the origin of the 'fine white stone from Sai' mentioned in 18th Dynasty texts.

Ethical approval

Ethical approval was not required for this study.

Use of AI tools

No artificial intelligence tools were used in the writing, analysis, or data handling for this manuscript.

Originality

This manuscript is original and has not been published or submitted elsewhere, in whole or in part.

All authors have read and approved the final version of the manuscript and agree with its submission to the Journal of Archaeological Science: Reports.

Funding

This study was written during the ERC DiverseNile project, which received funding from the European Research Council (ERC) under the European Union's Horizon 2020 research and innovation programme (grant agreement No. 865463).

CRediT authorship contribution statement

Fabian Dellefant: Writing – review & editing, Writing – original draft, Visualization, Methodology, Investigation, Formal analysis, Conceptualization. **Rosemarie Klemm:** Validation, Conceptualization. **Julia Budka:** Writing – review & editing, Writing – original draft, Validation, Supervision, Project administration, Investigation, Funding acquisition, Conceptualization. **Melanie Kaliwoda:** Writing – review & editing, Writing – original draft.

Declaration of competing interest

The authors declare that they have no known competing financial interests or personal relationships that could have appeared to influence the work reported in this paper.

Acknowledgments and Funding

We thank the constructive comments of three anonymous reviewers and the editorial handling of Ellery Frahm. This study was written during the ERC DiverseNile project, which received funding from the European Research Council (ERC) under the European Union's Horizon 2020 research and innovation programme (grant agreement No. 865463). The sandstone samples were exported to Munich during the ERC AcrossBorders project with the kind permission of the National Corporation for Antiquities and Museums of Sudan (NCAM). Sincere thanks are due in particular to Abdelrahman Ali Mohamed (Director General in 2016) and El-Hassan Ahmed Mohamed (Director of Fieldwork in 2016). The Raman spectroscopy measurement times, provided by and performed at the MSM Raman Lab (SNSB), are gratefully acknowledged. We thank Ingrid Carita Augustsson for helpful comments on the manuscript and are grateful to Chloë Ward (DiverseNile project) for improving our written English.

This publication honors Dietrich D. Klemm, whose work and dedication, alongside his wife Rosemarie Klemm, have significantly enriched our understanding of ancient Egypt. Their extensive research, particularly in the field of ancient Egyptian quarrying and mining, has shed invaluable light on the materials, techniques, and socio-economic aspects of the civilization. Through meticulous fieldwork, analysis, and scholarship, they have contributed to a deeper knowledge of Egypt's monumental achievements and the natural resources that played a crucial role in its development. Their joint efforts have left a lasting impact on the study of ancient Egypt's material culture and engineering practices.

Data availability

Data will be made available on request.

References

Geological Research Authority of Sudan (2005). Geological map of Sudan. 1: 3,500,000, Geological Research Authority of the Sudan, Khartoum.

Anand, R.R., Gilkes, R.J., 1984. Weathering of ilmenite in a lateritic pallid zone. Clays Clay Miner. 32, 363–374. https://doi.org/10.1346/CCMN.1984.0320504.

Azim, M., Carlotti, J.-F., 2012. Le temple a de l'île de Saï et ses abords. Cahiers De Recherches De L'institut De Papyrologie et D'égyptologie De Lille 29, 11–65.

Basu, A., Young, S.W., Suttner, L.J., James, W.C., Mack, G.H., 1975. Re-evaluation of the use of undulatory extinction and polycrystallinity in detrital quartz for provenance interpretation. J. Sediment. Petrol. 45, 873–882. https://doi.org/10.1306/212F6E6F-2B24-11D7-8648000102C1865D.

Bauer, M., Davydovskaya, P., Janko, M., Kaliwoda, M., Petersen, N., Gilder, S.A., Stark, R.W., 2011. Raman spectroscopy of laser-induced oxidation of titanomagnetites. J. Raman Spectrosc. 42, 1413–1418. https://doi.org/10.1002/jrs.2849.

Bentabol, M., Ruiz Cruz, M.D., Huertas, F.J., Linares, J., 2003. Hydrothermal transformation of kaolinite to illite at 200 and 300 °C. Clay Miner. 38, 161–172. https://doi.org/10.1180/0009855033820086.

Berger, G., Lacharpagne, J.C., Velde, B., Beaufort, D., Lanson, B., 1997. Kinetic constraints on illitization reactions and the effects of organic diagenesis in sandstone/shale sequences. Appl. Geochem. 12, 23–35. https://doi.org/10.1016/S0883-2927(96)00051-0.

Blenkinsop, T., 2002. Deformation Microstructures and Mechanisms in Minerals and Rocks, Deformation Microstructures and Mechanisms in Minerals and Rocks. Kluwer Academic Publishers, Dordrecht.

Budka, J. (Ed.), 2017. AcrossBorders I: The New Kingdom Town of Sai Island, Sector SAV1 North. Contributions to the Archaeology of Egypt, Nubia and the Levant 4, Austrian Academy of Sciences, Vienna. https://doi.org/10.2307/j.ctt1vjqpq9.

Budka, J., 2020. AcrossBorders 2: Living in New Kingdom Sai. With contributions by Johannes Auenmüller, Annette. In: Archaeology of Egypt, Sudan and the Levant 1. Austrian Academy of Sciences Press, Vienna. https://doi.org/10.1553/0x003b4640.

Budka, J., 2024. Regional perspectives on resource management in the Middle Nile, in: Budka, J., Lemos, R. (Eds.), Landscape and Resource Management in Bronze Age Nubia: Archaeological Perspectives on the Exploitation of Natural Resources and the Circulation of Commodities in the Middle Nile. Contributions to the Archaeology of Egypt, Nubia and the Levant 17, Harrassowitz, Wiesbaden, pp. 19–33.

Chamley, H., 1989. Clay Sedimentology. Springer, Berlin Heidelberg.

Cuadros, J., Vega, R., Toscano, A., Arroyo, X., 2014. Kaolinite transformation into dickite during burial diagenesis. Am. Mineral. 99, 681–695. https://doi.org/10.2138/am.2014.4614.

de Faria, D.L.A., Lopes, F.N., 2007. Heated goethite and natural hematite: can Raman spectroscopy be used to differentiate them? Vib. Spectrosc 45, 117–121. https://doi.org/10.1016/j.vibspec.2007.07.003.

Deaton, B.C., 1987. Quantification of rock color from Munsell chips. J. Sediment. Res. 57, 774–776. https://doi.org/10.1306/212F8C33-2B24-11D7-8648000102C1865D.

Deer, W.A., Howie, R.A., Zussman, J., 2013. An Introduction to the Rock-Forming Minerals, third ed. Berforts Information Press, Stevenage, Hertfordshire.

Dellefant, F., Trepmann, C.A., Schmahl, W.W., Gilder, S.A., Sleptsova, I.V., Kaliwoda, M., 2024. Ilmenite phase transformations in suevite from the Ries impact structure (Germany) record evolution in pressure, temperature, and oxygen fugacity conditions. Am. Mineral. 109, 1005–1023. https://doi.org/10.2138/am-2023-8985.

Devauchelle, D., Doyen, F., 2009. Retour á l'Ile de Saï (Soudan, 2006-2009). Bull. La Société Française D'égyptologie 175, 29–49.

Dill, H.G., 2016. Kaolin: Soil, rock and ore: from the mineral to the magmatic, sedimentary and metamorphic environments. Earth-Science Rev. 161, 16–129. https://doi.org/10.1016/j.earscirev.2016.07.003.

Dott, R.H.J., 1964. Wacke, graywacke and matrix - what approach to immature sandstone classification? J. Sediment. Petrol. 34, 625–632. https://doi.org/10.1306/74D71109-2B21-11D7-8648000102C1865D.

Draganits, E., 2014. Geoarchaeological investigations on Sai Island (Sudan). Rapp. AcrossBorders Geoarchaeological Fieldwork. 10.13140/RG.2.2.24775.70563.

Ehrenberg, S.N., 1989. Formation of Diagenetic Illite in Sandstones of the Garn Formation, Haltenbanken Area, Mid-Norwegian Continental Shelf. Clay Miner. 24, 233–253. https://doi.org/10.1180/claymin.1989.024.2.09.

Ehrenberg, S.N., Aagaard, P., Wilson, M.J., Fraser, A.R., Duthie, D.M.L., 1993. Depth-Dependent Transformation of Kaolinite to Dickite, In: Sandstones of the Norwegian Continental Shelf. Clay Miner. 28, 325–352. 10.1180/claymin.1993.028.3.01.

Elgendy, N.T.H., Abuamarah, B.A., Nabawy, B.S., Ghrefat, H., Kassem, O.M.K., 2020. Pore fabric anisotropy of the Cambrian–Ordovician Nubia Sandstone in the Onshore Gulf of Suez, Egypt: a Surface Outcrop Analog. Nat. Resour. Res. 29, 1307–1328. https://doi.org/10.1007/s11053-019-09520-6.

Garcea, E.A.A., Hildebrand, E.A., 2009. Shifting social networks along the Nile: Middle Holocene ceramic assemblages from Sai Island, Sudan. J. Anthropol. Archaeol. 28, 304–322. https://doi.org/10.1016/j.jaa.2009.05.002.

Ghiorso, M.S., Sack, O., 1991. Fe-Ti oxide geothermometry: thermodynamic formulation and the estimation of intensive variables in silicic magmas. Contrib. to Mineral. Petrol. 108, 485–510. https://doi.org/10.1007/BF00303452.

Grey, I.E., Reid, A.F., 1975. The structure of Pseudorutile and its role in the natural alteration of llmenite. Am. Mineral. 60, 898–906.

Gupta, S.K., Rajakumar, V., Grieveson, P., 1991. Phase transformations during heating of llmenite concentrates. Metall. Trans. B 22, 711–716. https://doi.org/10.1007/BF02679027.

Harrell, J.A., 2024. Archaeology and Geology of Ancient Egyptian Stones (2 Vol.). Archaeopress Publishing Ltd, Oxford.

Hong, H., Cheng, F., Yin, K., Churchman, G.J., Wang, C., 2015. Three-component mixed-layer illite/smectite/kaolinite (I/S/K) minerals in hydromorphic soils, south China. Am. Mineral. 100, 1883–1891. https://doi.org/10.2138/am-2015-5170.

Hou, T., Botcharnikov, R., Moulas, E., Just, T., Berndt, J., Koepke, J., Zhang, Z., Wang, M., Yang, Z., Holtz, F., 2021. Kinetics of Fe-Ti Oxide Re-equilibration in Magmatic Systems: Implications for Thermo-oxybarometry. J. Petrol. 61, 1–24. https://doi.org/10.1093/petrology/egaa116.

Huang, W.L., Bishop, A.M., Brown, R.W., 1986. The effect of fluid/rock ratio on feldspar dissolution and illite formation under reservoir conditions. Clay Miner. 21, 585–601. https://doi.org/10.1180/claymin.1986.021.4.10.

Huertas, F.J., Fiore, S., Huertas, F., Linares, J., 1999. Experimental study of the hydrothermal formation of kaolinite. Chem. Geol. 156, 171–190. https://doi.org/10.1016/S0009-2541(98)00180-6.

Imperial, A., Pe-Piper, G., Piper, D.J.W., Grey, I.E., 2022. Identifying pseudorutile and Kleberite using Raman spectroscopy. Minerals 12, 1210. https://doi.org/10.3390/min12101210.

Janoo, V.C., 1998. Quantification of shape, angularity, and surface texture of base course materials. CRREL Spec. Rep. 98–1 22, pp.

Klemm, D.D., Klemm, R., 2001. The building stones of ancient Egypt - a gift of its geology. J. African Earth Sci. 33, 631–642. https://doi.org/10.1016/s0899-5362(01)00085-9.

Klemm, R., Klemm, D.D., 2008. Stones and quarries in ancient Egypt. British Museum Press, London.

Lanson, B., Beaufort, D., Berger, G., Bauer, A., Cassagnabère, A., Meunier, A., 2002. Authigenic kaolin and illitic minerals during burial diagenesis of sandstones: a review. Clay Miner. 37, 1–22. https://doi.org/10.1180/0009855023710014.

Lattard, D., Partzsch, G.M., 2001. Magmatic crystallization experiments at 1 bar in systems closed to oxygen: a new/old experimental approach. Eur. J. Mineral. 13, 467–478. https://doi.org/10.1127/0935-1221/2001/0013-0467.

Lattard, D., Sauerzapf, U., Käsemann, M., 2005. New calibration data for the Fe-Ti oxide thermo-oxybarometers from experiments in the Fe-Ti-O system at 1 bar, 1,000-1,300°C and a large range of oxygen fugacities. Contrib. to Mineral. Petrol. 149, 735–754. https://doi.org/10.1007/s00410-005-0679-2.

Lewis, J., Smith, J., Garcea, E., 2011. Paleoenvironmental implications of the isotope geochemistry and granulometry of Quaternary alluvial sediments and paleosols from Sai Island, Sudan, in: GSA Annual Meeting. Minneapolis, p. abstract, 95-1.

Lindsley, D.H., 1991. Experimental studies of oxide minerals, in: Lindsley, D.H. (Ed.), Oxide Minerals: Petrologic and Magnetic Significance. Mineralogical Society of America, Washington D.C., pp. 69–106. 10.1515/9781501508684-006.

Mazza, T., Barborini, E., Piseri, P., Milani, P., Cattaneo, D., Li Bassi, A., Bottani, C.E., Ducati, C., 2007. Raman spectroscopy characterization of TiO2 rutile nanocrystals. Phys. Rev. B - Condens. Matter Mater. Phys. 75, 1–5. https://doi.org/10.1103/PhysRevB.75.045416.

McKeown, D.A., Bell, M.I., Etz, E.S., 1999. Vibrational analysis of the dioctahedral mica: 2M1 muscovite. Am. Mineral. 84, 1041–1048. https://doi.org/10.2138/am-1999-7-806.

Merino, E., Nahon, D., Wang, Y., 1993. Kinetics and mass transfer of pseudomorphic replacement application to replacement of parent materials and kaolinite by Al Fe and Mn oxides during weathering. Am. J. Sci. 293, 135–155. https://doi.org/10.2475/ajs.293.2.135.

Mücke, A., Bhadra Chaudhuri, J.N., 1991. The continuous alteration of ilmenite through pseudorutile to leucoxene. Ore Geol. Rev. 6, 25–44. https://doi.org/10.1016/0169-1368(91)90030-B.

Nabawy, B.S., Abdelhalim, A., El-Meselhy, A., 2019. Step-drawdown test as a tool for the assessment of the Nubia sandstone aquifer in East El-Oweinat Area, Egypt. Environ. Earth Sci. 78, 375. https://doi.org/10.1007/s12665-019-8375-0.

Nabawy, B.S., Khalil, H.M., Fathy, M.S., Ali, F., 2020. Impacts of microfacies type on reservoir quality and pore fabric anisotropy of the Nubia sandstone in the central Eastern Desert, Egypt. Geol. J. 55, 4507–4524. https://doi.org/10.1002/gj.3690.

Nabawy, B.S., Rochette, P., Géraud, Y., 2010. Electric pore fabric of the Nubia sandstones in south Egypt: characterization and modelling. Geophys. J. Int. 183, 681–694. https://doi.org/10.1111/j.1365-246X.2010.04789.x.

Ohsaka, T., Izumi, F., Fujiki, Y., 1978. Raman spectrum of anatase, TiO_2. J. Raman Spectrosc. 7, 321–324. https://doi.org/10.1002/jrs.1250070606.

Pettijohn, F.J., Potter, P.E., Siever, R., 1987. Sand and Sandstone, second ed. Springer, New York.

Pomeyrol, R., 1968. Nubian Sandstone. Am. Assoc. Pet. Geol. Bull. 589–600.

Rogers, J.J.W., Head, W.B., 1961. Relationships between porosity, median size, and sorting coefficients of synthetic sands. J. Sediment. Res. 31. https://doi.org/10.1306/74D70BA5-2B21-11D7-8648000102C1865D.

Sass, B.M., Rosenberg, P.E., Kittrick, J.A., 1987. The stability of illite/smectite during diagenesis: an experimental study. Geochim. Cosmochim. Acta 51, 2103–2115. https://doi.org/10.1016/0016-7037(87)90259-6.

Sauerzapf, U., Lattard, D., Burchard, M., Engelmann, R., 2008. The titanomagnetite-ilmenite equilibrium: New experimental data and thermo-oxybarometric application to the crystallization of basic to intermediate rocks. J. Petrol. 49, 1161–1185. https://doi.org/10.1093/petrology/egn021.

Shah, B.A., Bandyopadhyay, D.N., 2005. Feldspar alteration and diagenetic characteristics of the Parsora sandstones, Son Basin. India. Gondwana Res. 8, 258–265. https://doi.org/10.1016/S1342-937X(05)71124-2.

Singer, A., 1980. The paleoclimatic interpretation of clay minerals in soils and weathering profiles. Earth Sci. Rev. 15, 303–326. https://doi.org/10.1016/0012-8252(80)90113-0.

Spence, K., Rose, P., Bunbury, J., Clapham, A., Collet, P., Smith, G., Soderberg, N., 2009. Fieldwork at Sesebi, 2009. Sudan & Nubia 13, 38–46.

Temple, A.K., 1966. Alteration of ilmenite. Econ. Geol. 61, 695–714. https://doi.org/10.2113/gsecongeo.61.4.695.

Teufer, G., Temple, A.K., 1966. Pseudorutile—a New Mineral Intermediate between Ilmenite and Rutile in the N Alteration of Ilmenite. Nature 211, 179–181. https://doi.org/10.1038/211179b0.

Thurmond, A.K., Stern, R.J., Abdelsalam, M.G., Nielsen, K.C., Abdeen, M.M., Hinz, E., 2004. The Nubian Swell. J. African Earth Sci. 39, 401–407. https://doi.org/10.1016/j.jafrearsci.2004.07.027.

Trepmann, C.A., Dellefant, F., Kaliwoda, M., Hess, K.U., Schmahl, W.W., Hölzl, S., 2020. Quartz and cristobalite ballen in impact melt rocks from the Ries impact structure,

Germany, formed by dehydration of shock-generated amorphous phases. Meteorit. Planet. Sci. 55, 2360–2374. https://doi.org/10.1111/maps.13590.
Ullmann, M., 2020. Textual sources for sandstone from Sai, in: Budka, J., AcrossBorders 2: Living in New Kingdom Sai. Austrian Academy of Sciences Press, Vienna, pp. 52–53.
Ulmer-Scholle, D.S., Scholle, P.A., Schieber, J., Raine, R.J., 2015. Sand & Sandstone Textures, in: A Color Guide to the Petrography of Sandstones, Siltstones, Shales and Associated Rocks. American Association of Petroleum Geologists, pp. 147–166. 10.1306/13521909M1093637.
Van Peer, P., Fullagar, R., Stokes, S., Bailey, R.M., Moeyersons, J., Steenhoudt, F., Geerts, A., Vanderbeken, T., De Dapper, M., Geus, F., 2003. The Early to Middle Stone Age transition and the emergence of modern human behaviour at site 8-B-11 Sai Island, Sudan. J. Hum. Evol. 45, 187–193. https://doi.org/10.1016/S0047-2484(03)00103-9.
Vercoutter, J., 1986. Préface: l'archéologie de l'île de Saï, in: Gratien, B., Saï I. La Nécropole Kerma, Centre National de la Recherche Scientfique Mission, Archeologique Francaise au Soudan, Institut de Papyrologie et d'Egyptologie de l'Universite de Lille III, Paris, pp. 7–17.
Vercoutter, J., 1958. Excavations at Sai 1955–7: a preliminary report. Kush J. Sudan Antiq. Serv. 6, 144–169.
Wang, A., Freeman, J.J., Jolliff, B.L., 2015. Understanding the Raman spectral features of phyllosilicates. J. Raman Spectrosc. 46, 829–845. https://doi.org/10.1002/jrs.4680.
Wang, A., Kuebler, K.E., Jolliff, B.L., Haskin, L.A., 2004. Raman spectroscopy of Fe-Ti-Cr-oxides, case study: Martian meteorite EETA79001. Am. Mineral. 89, 665–680. https://doi.org/10.2138/am-2004-5-601.
White, A.F., Bullen, T.D., Schulz, M.S., Blum, A.E., Huntington, T.G., Peters, N.E., 2001. Differential rates of feldspar weathering in granitic regoliths. Geochim. Cosmochim. Acta 65, 847–869. https://doi.org/10.1016/S0016-7037(00)00577-9.
Yuan, G., Cao, Y., Schulz, H.M., Hao, F., Gluyas, J., Liu, K., Yang, T., Wang, Y., Xi, K., Li, F., 2019. A review of feldspar alteration and its geological significance in sedimentary basins: from shallow aquifers to deep hydrocarbon reservoirs. Earth-Science Rev. 191, 114–140. https://doi.org/10.1016/j.earscirev.2019.02.004.
Zotov, A., Mukhamet-Galeev, A., Schott, J., 1998. An experimental study of kaolinite and dickite relative stability at 150-300 °C and the thermodynamic properties of dickite. Am. Mineral. 83, 516–524. https://doi.org/10.2138/am-1998-5-611.